NJC

Accepted Manuscript

This is an *Accepted Manuscript*, which has been through the Royal Society of Chemistry peer review process and has been accepted for publication.

Accepted Manuscripts are published online shortly after acceptance, before technical editing, formatting and proof reading. Using this free service, authors can make their results available to the community, in citable form, before we publish the edited article. We will replace this *Accepted Manuscript* with the edited and formatted *Advance Article* as soon as it is available.

You can find more information about *Accepted Manuscripts* in the Information for Authors.

Please note that technical editing may introduce minor changes to the text and/or graphics, which may alter content. The journal's standard Terms & Conditions and the Ethical guidelines still apply. In no event shall the Royal Society of Chemistry be held responsible for any errors or omissions in this *Accepted Manuscript* or any consequences arising from the use of any information it contains.

ROYAL SOCIETY OF CHEMISTRY

www.rsc.org/njc

Hybridization of zirconia, zinc and iron supported on HY zeolite as solar-based catalyst for rapid decolorization of various dyes

Norzahir Sapawe

Section of Technical Foundation, Universiti Kuala Lumpur – Malaysian Institute of Chemical and Bioengineering Technology, Lot 1988 Vendor City, Taboh Naning, 78000 Alor Gajah, Melaka, MALAYSIA.

*To whom correspondence should be addressed,
Norzahir Sapawe (Ph.D.)
Tel : +6013-575-7795 Fax: +606-551-2001
Email : norzahir@unikl.edu.my ; za_heer86@yahoo.com

Abstract

Hybridization of an electrogenerated zirconia/zinc/iron–supported on HY zeolite nanocomposite catalyst ($EGZrO_2$/EGZnO/$EGFe_2O_3$/HY) was prepared by a facile one–pot electrochemical method. In this study, nanoparticles (<35 nm in size) of electrogenerated zirconia oxide ($EGZrO_2$), electrogenerated zinc oxide (EGZnO), and electrogenerated iron oxide ($EGFe_2O_3$) were formed and distributed on the surface of the HY support. The photoactivity of the catalyst was examined in the photodecolorization of methylene blue (MB) under varying pH, catalyst dosages, and initial concentrations of MB. An amount of 0.38 g L^{-1} 1 wt% $EGZrO_2$/1 wt% EGZnO/1 wt% $EGFe_2O_3$/HY was found to be the optimum dosage for 10 mg L^{-1} MB, which gave complete decolorization of MB after 1 h of contact time at pH 9 under sunlight irradiation. This result confirmed the high photoactivity of the catalyst compared to other single or double nanometal oxide–supported HY catalysts studied. Nearly complete mineralization of MB was observed, and the catalyst was still stable after six cycling runs with a negligible leaching effect. Significantly, a high decolorization percentage (>80%) of other dyes such as malachite green (MG), congo red (CR), disperse violet (DV), and disperse blue (DB) were obtained when using this promising electrogenerated nanocomposite catalyst.

Keywords**:** nanocomposite catalyst, $EGZrO_2$/EGZnO/$EGFe_2O_3$/HY, electrochemical, photodecolorization, methylene blue

1. Introduction

Advanced oxidation processes (AOPs) using semiconductors such as TiO_2, ZnO, WO_3, Fe_2O_3, CuO, ZrO_2, and CdS as photocatalysts are an essential technique in wastewater treatment because they can convert a wide range of harmful dyes at ambient temperature into non–toxic products, CO_2 and water [1–3]. The mixed metal oxides such as TiO_2–ZrO_2, Ag–ZnO, Fe_2O_3–TiO_2, Sn–ZnO, Ag–TiO_2, and ZnO–ZrO_2 have also been recognized to exhibit better performance and enhanced photocatalytic activity [4–9]. However, few studies have been reported based on the use of more than two metal oxides as the photocatalyst.

Intensive research using the mesoporous materials such as zeolite as a support for metal oxides such as TiO_2–HZSM5, Co–ZSM5, and CuO–X has become the focus among researchers because they influence the catalytic performance through structural features [10–12]. Zeolitic materials offer a high surface area, are thermally stable, eco–friendly, and also specific photophysical properties in controlling the charge and electron transfer processes [13–14]. The interaction between the zeolite and metal oxide also leads to an enhancement in the contact between the catalyst surface and irradiation, as well as less amount of metal oxides was required [15].

Recently, we have reported a new preparation method for an α–Fe_2O_3, EGZrO_2, EGZnO, and CuO supported HY catalyst by a simple and rapid electrochemical process, which possesses high photoactivity in the decolorization of various synthetic dyes [1–3,16]. The nanosized metal oxides as well as the synergistic interaction between the metal and the support were found to play important roles in the enhancement of the reaction [17–18]. The introduction of several metal oxides presumably could be improved and endowed extra properties to the photocatalyst by altering and restructuring the materials [4]. Thus, we attempted to prepare ZrO_2, ZnO, and Fe_2O_3 supported on HY zeolite by the corresponding method. ZrO_2 was chosen due to its

specific optical and electrical properties, thermal stability, and strong mechanical strength as well as the presence of acid–base and redox capabilities [19,20], while ZnO has attracted much attention due to its similar band gap energy to TiO_2 (3.20 eV) which possesses high photosensitivity and the ability to degrade various pollutants [5,21].

Therefore, we report for the first time, the facile synthesis of electrogenerated nanoparticles of a Zr, Zn, and Fe–supported HY ($EGZrO_2$/EGZnO/$EGFe_2O_3$/HY) catalyst, and its remarkable performance toward the photodecolorization of methylene blue (MB). The 1 wt% $EGZrO_2$/1 wt% EGZnO/1 wt% $EGFe_2O_3$/HY was electrosynthesized within less than 6 min. The catalysts were then characterized by X–ray diffraction (XRD), transmission electron microscopy (TEM), Brunnauer–Emmett–Teller surface area analysis (BET), and inductively coupled plasma mass spectrometry (ICP–MS). The performance of $EGZrO_2$/EGZnO/$EGFe_2O_3$/HY was compared with bare HY, $EGZrO_2$/HY, EGZnO/HY, $EGFe_2O_3$/HY, $EGZrO_2$/EGZnO/HY, $EGZrO_2$/$EGFe_2O_3$/HY, and EGZnO/$EGFe_2O_3$/HY catalysts. The appropriate conditions for photodecolorization were examined under varying pH, catalyst dosages, and initial concentrations of MB. The kinetic behavior of the catalyst was also studied to determine the surface interaction of the catalyst with MB. In this work, a new model of the $EGZrO_2$/EGZnO/$EGFe_2O_3$/HY nanocomposite catalyst was prepared using a simple operation within a short reaction time to give a high decolorization percentage of MB, thus endowing this catalyst with the potential to be used as a promising photocatalyst.

2. Experimental

2.1. Materials

The HY zeolite had a Si/Al ratio of 80 and was purchased from Zeolyst International. *N,N*–dimethylformamide (DMF) was purchased from Merck and naphthalene was obtained from Fluka. Sodium hydroxide, hydrochloric acid, and methylene blue (C.I. 52015 for microscopy) were obtained from QReC^{TM}. The platinum (Pt), zirconia (Zr), zinc (Zn), iron (Fe) plate cells were obtained from Nilaco Metal, Japan. All reagents were of analytical grade and were used as received. Deionized water was used for the preparation of the pH solution and adjustments to the pH were performed using a 0.1M HCl and NaOH solution.

2.2. Catalyst preparation

The 1 wt% EGZrO_2/1 wt% EGZnO/1 wt% EGFe_2O_3/HY catalyst was prepared according to the previously reported procedure [2,9,16]. A 10 mL DMF solution containing 0.1 M tetraethylammonium perchlorate was electrolyzed in the presence of 6 mmol naphthalene as a mediator and 1.5 g HY zeolite in a normal one–compartment cell fitted with a Pt plate cathode (2 × 2 cm^2) and Zr, Zn, and Fe anode plates (2 × 2 cm^2 each) at a constant current density of 120 mA/cm^2 under a nitrogen atmosphere at 273 K. The anodes were used alternately as Zr, Zn and Fe, depending on the amount required. After electrolysis the mixture was impregnated, oven dried overnight at 378 K, and calcined at 823 K for 3 h to yield a brownish powder EGZrO_2/EGZnO/EGFe_2O_3/HY catalyst, which ready for characterization and photocatalytic testing.

The bare nanoparticles EGZrO_2, EGZnO, and EGFe_2O_3 were prepared using the same procedure as above but in the absence of HY zeolite. The required weight percent of the EGZrO_2, EGZnO, and EGFe_2O_3 supported on HY was calculated by the time of electrolysis, which is based on the Faraday's law,

$$t = \left(\frac{F}{I}\right)(z \times n) \quad (1)$$

where t = total time for the constant current applied (s); F = 96486 C mol^{-1}, which is the Faraday constant; I = the electric current applied (mA); z = the valency number of ions of substance (electrons transferred per ion); and n = the number of moles of substance (number of moles, liberated n = m/M).

2.3. Characterization

The crystalline structures of the catalysts were studied by XRD recorded on a D8 ADVANCE Bruker X–ray diffractometer using Cu K_α radiation at a 2θ angle ranging from 3° to 90°. The particle sizes of the catalysts were calculated using the Debye–Scherrer equation,

$$D = \frac{k\lambda}{\beta \cos\theta} \quad (2)$$

where k = 0.94 is a coefficient, λ = 1.5406 Å is the X–ray wavelength, β is the full width half maximum (FWHM) of the sample and θ is the diffracting angle. The phases were identified with the aid of the Joint Committee on Powder Diffraction Standards (JCPDS) files.

The morphological properties of the $EGZrO_2$/EGZnO/$EGFe_2O_3$/HY nanocomposite catalyst as well as the distribution of $EGZrO_2$/EGZnO/$EGFe_2O_3$ deposited on the HY surface were examined by TEM (JEOL JEM–2100F). The textural properties (i.e., specific surface area, pore volume, and pore diameter) were determined from nitrogen adsorption–desorption

isotherms at liquid nitrogen temperature using a Micromeritics ASAP 2010 instrument. The surface area was calculated with the BET method, and pore distributions were determined by the Barrett–Joyner–Halender (BJH) method. Prior to measurement, all the samples were degassed at 383 K to 0.1 Pa. The band gap energy of $EGZrO_2$, EGZnO, $EGFe_2O_3$, $EGZrO_2$/EGZnO/$EGFe_2O_3$, and $EGZrO_2$/EGZnO/$EGFe_2O_3$/HY was determined from plots of the Kubelka–Munk (K–M) function [$f_{K\text{-}M} = (h\nu/\lambda)^{1/2}$] as a function of the energy of the excitation light [hν].

2.4. Photocatalytic testing

The photocatalytic activity of the prepared $EGZrO_2$/EGZnO/$EGFe_2O_3$/HY catalyst was tested for the decolorization of MB. A 0.08 g of the catalyst was dispersed in 200 mL of 10 mg L^{-1} MB aqueous solution. The adsorption–desorption equilibrium was achieved under dark conditions after 1 h, and the mixture was then exposed for 1 h with constant stirring under sunlight (January to March 2014, between 12 NN until 3 PM). The average intensity of sunlight during this period is 1.315 x 10^5 Lux unit. Irradiation was carried out in the open air condition. However, during the illumination time, no volatility of the solvent was observed.

At specific time intervals, 2.5 mL of the sample solution was withdrawn and centrifuged prior measurements for the remaining MB concentration by a UV–vis spectrophotometer (Thermo Scientific Genesys 10 uv Scanning) using the characteristic adsorption band at 664 nm. The decolorization percentage was calculated as follows,

$$Decolorization\ (\%) = \frac{(C_0 - C_t)}{C_0} \times 100 \quad (3)$$

where C_o represents the initial concentration and C_t denotes a variable concentration.

2.5. Analyses

The elemental analyses of Zr, Zn, and Fe in a solution during an experiment were determined by ICP–MS using ELAN 6100 Perkin Elmer ICPMS. The BOD of the solution were measured using YSI model 33, whereas the BOD bottles were incubated at 293 K for five days and the difference in dissolved oxygen was used to calculate BOD_5. The HACH DR4000 spectrometer was used for COD measurement. In addition, the total organic carbon (TOC) removal was determined using a TOC Shimadzu Vcph spectrophotometer for each run before and after a 1 h reaction time for the evaluation of the mineralization of MB dye. TOC was calculated as the difference between the total carbon (TC) and inorganic (IC) in the liquid sample.

3. Results and Discussion

3.1. Characterization

3.1.1 Crystallinity, phase and structural studies

The XRD pattern of the prepared catalysts was compared, and the results are shown in Fig. 1. According to Fig. 1a, the peak intensity of HY decreased as the $EGZrO_2$, EGZnO, and $EGFe_2O_3$ were loaded onto HY, suggesting that the presence of foreign substances affected the morphology of the supported HY fingerprint. Almost all of the peaks corresponding to $EGZrO_2$,

194 EGZnO, and $EGFe_2O_3$ were detected in $EGZrO_2$/EGZnO/$EGFe_2O_3$ nanocomposite, indicating

195 that the prepared catalysts were well−mixed (Fig. 1b).

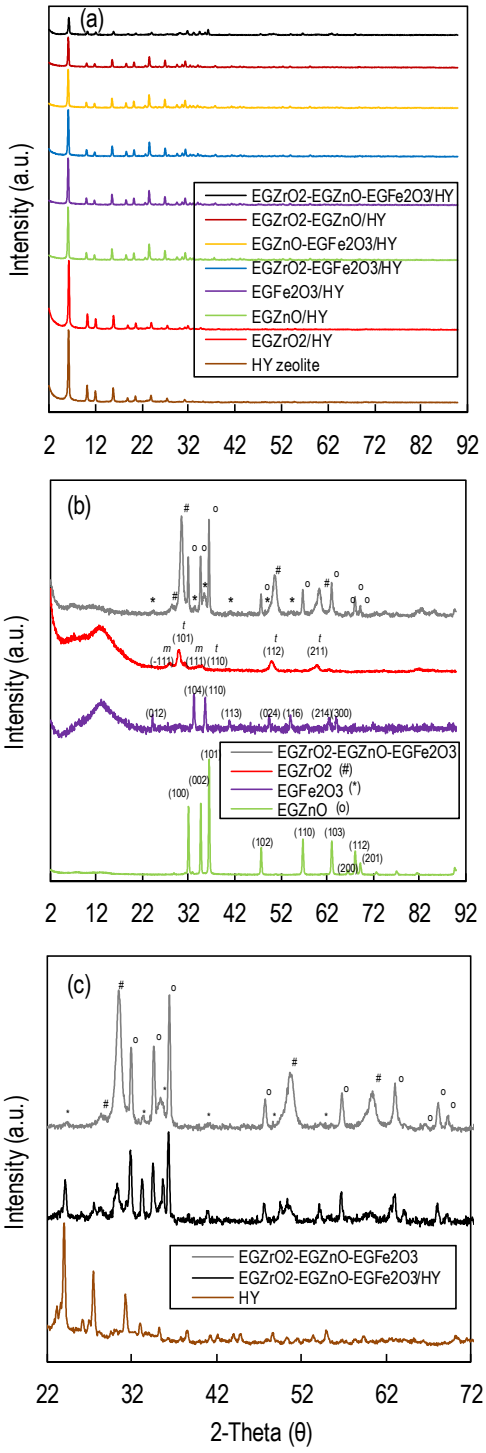

196

197 Fig. 1. XRD patterns of catalysts (a) and (b) for full range 2–92^0 and (c) for range 22–72^0

198 A series of peaks were observed for $EGZrO_2$, EGZnO, and $EGFe_2O_3$, which are consistent
199 with the tetragonal and monoclinic phase of ZrO_2 (JCPDS 36–1541), the hexagonal wurtzite
200 structure of ZnO (JCPDS 36−1541), and the hematite phase of $\alpha-Fe_2O_3$ with rhombohedral
201 symmetry (JCPDS 33–0664), respectively, with no other diffraction peaks being detected,
202 indicating the purity of the prepared catalysts [1,16,21,22].
203 Fig. 1c shows the enlargement of a selected area of the XRD pattern from 22º to 72º for
204 $EGZrO_2$/EGZnO/$EGFe_2O_3$, $EGZrO_2$/EGZnO/$EGFe_2O_3$/HY, and bare HY. There were several
205 peaks detected corresponding to ZrO_2, ZnO, and Fe_2O_3, verifying the presence of $EGZrO_2$,
206 EGZnO, and $EGFe_2O_3$ metals on the HY support.
207 The average crystallite size of the catalysts was estimated by the Debye–Scherrer equation
208 on the basis of the major peaks of $EGZrO_2$ (101), EGZnO (101), and $EGFe_2O_3$ (104), which
209 were 11.7 nm, 30.2 nm, and 26.5 nm, respectively. However, this crystallite size was increased
210 to 13.6 nm, 32.8 nm, and 28.5 nm, respectively, upon the formation of the nanocomposite
211 $EGZrO_2$/EGZnO/$EGFe_2O_3$ catalyst. This may be due to agglomeration and the interaction
212 between the zirconia, zinc, and iron species [23].
213
214 *3.1.2 Morphological properties*
215
216 The morphological properties of the $EGZrO_2$/EGZnO/$EGFe_2O_3$/HY catalysts were
217 examined by HR–TEM, and the images are presented in Fig. 2. The inset image shows the fast
218 Fourier transform patterns (FFT), and magnification of the selected area in the FFT patterns
219 showed the atomic arrangement in the crystal, and allowed the estimation of the interplanar
220 distances. Figs. 2a, 2b, and 2c illustrate that the $EGZrO_2$, EGZnO, and $EGFe_2O_3$ nanoparticles
221 were successfully prepared with well–defined boundaries and no connecting necks, which
222 indicates the absence of a sintering effect between the particles.

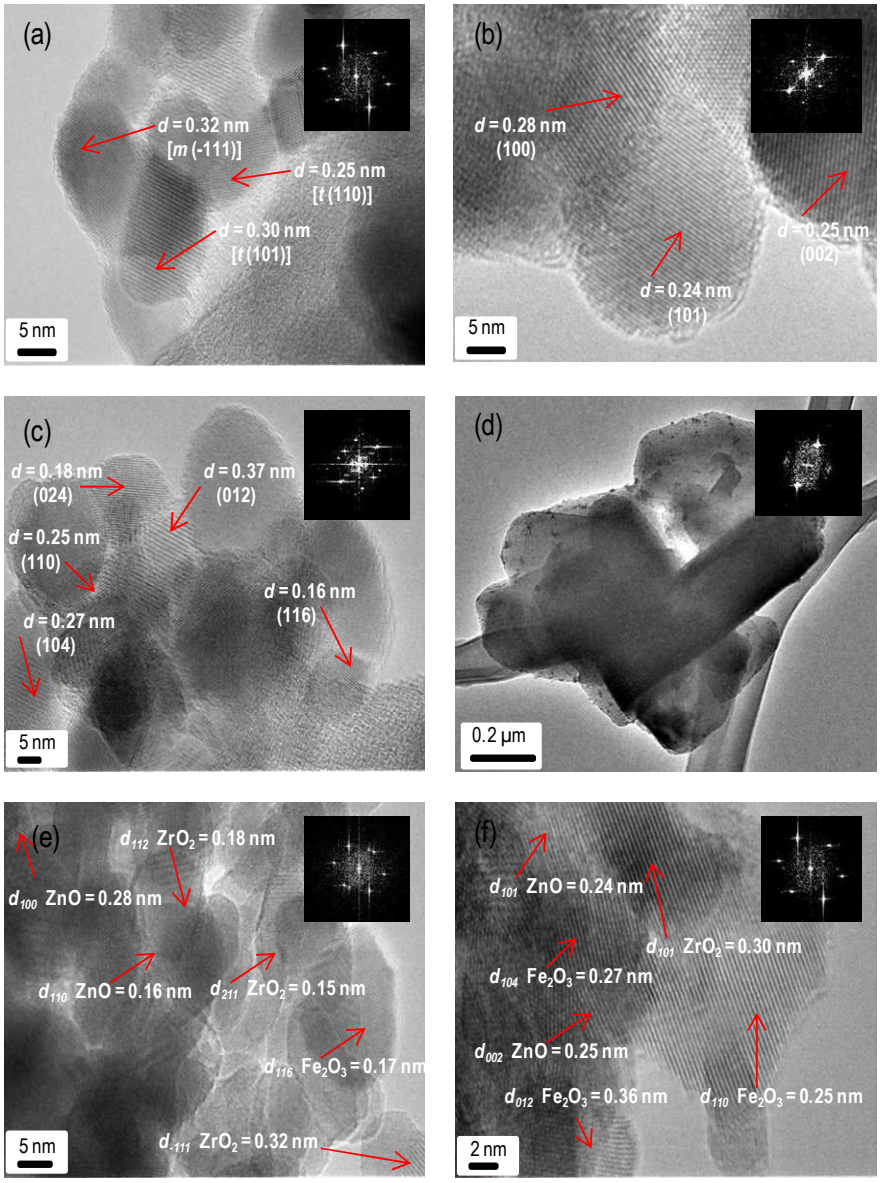

Fig. 2. HR–TEM micrographs of (a) $EGZrO_2$ (b) EGZnO (c) $EGFe_2O_3$ (d, e, and f) $EGZrO_2$/EGZnO/$EGFe_2O_3$/HY in low and high magnification and the insert of Fig. 2 are its corresponding FFT

The average particle size for $EGZrO_2$, EGZnO, and $EGFe_2O_3$ varied in a narrow range from 5–35 nm. The theoretical values of the particle sizes (*D*) were found to be 19.2 nm, 17.5 nm, and 22.9 nm, respectively, which were estimated by the following equation:

$$D = \frac{6}{\rho S} \quad (4)$$

where ρ is the theoretical density of the electrogenerated metal oxide powder and S is the surface area determined by N_2 adsorption–desorption isotherms, assuming that the particles are spherical in shape [24].

However, the micrographs show particles with an elliptical and irregular shape, which may be due to the particles overlapping [19]. The value of the interplanar distance (*d*–spacing) of the lattice fringes estimated from this image was consistent with the value of the lattice spacing of $EGZrO_2$, EGZnO, and $EGFe_2O_3$ which is available in the XRD database. Based on this result, it was confirmed that $EGZrO_2$, EGZnO, and $EGFe_2O_3$ existed in the HY support (Figs. 2d, 2e, and 2f).

3.1.3 Study of textural properties

The surface area analysis data obtained from the BET method as well as the pore volume and pore diameter determined by the Barret–Joyner–Halenda (BJH) desorption isotherms method were tabulated in Table 1. The addition of $EGZrO_2$/EGZnO/$EGFe_2O_3$ onto HY increased the surface area, pore diameter, and pore volume, which may have been due to the existence of electrogenerated metal oxide nanoparticles. The improvement in the surface contact of the catalyst enhanced the light irradiation, thereby increasing the photodecolorization of MB. A similar observation was also reported for the photoreduction of methyl orange by TiO_2 supported on a zeolite matrix [25].

Table 1. The textural properties of the catalysts

Catalysts	Surface area (m^2g^{-1})	Average pore diameter* (nm)	Pore volume (cm^3g^{-1})
$EGZrO_2$	54.9	11.1	0.153
EGZnO	61.3	6.37	0.263
$EGFe_2O_3$	50.1	3.81	0.053
$EGZrO_2/EGZnO/EGFe_2O_3$	163	5.13	0.352
HY	557	2.70	0.376
$EGZrO_2/EGZnO/EGFe_2O_3/HY$	636	2.90	0.462

*adsorption average pore diameter (4V/V by BET)

3.2. Photocatalytic testing for the decolorization of MB

3.2.1. Catalyst performance

The photoactivity of the prepared $EGZrO_2/EGZnO/EGFe_2O_3/HY$ catalyst was tested and compared with bare HY, Degussa P25 TiO_2, $EGZrO_2/HY$, EGZnO/HY, $EGFe_2O_3/HY$, $EGZrO_2/EGZnO/HY$, $EGZrO_2/EGFe_2O_3/HY$, and $EGZnO/EGFe_2O_3/HY$ catalysts on the decolorization of MB; the results are shown in Fig. 3. For comparison, a controlled experiment (known as photolysis) was also carried out without the presence of any catalyst. Each experiment was performed in the dark to achieve adsorption–desorption equilibrium before exposure to sunlight for 1 h with constant stirring. The results show that almost complete decolorization of MB was achieved within a short period (1 h) of contact time when using $EGZrO_2/EGZnO/EGFe_2O_3/HY$, compared with the other examined catalysts, indicating the high photoactivity of the prepared nanocomposite catalyst under sunlight irradiation. Under photolysis conditions, only 3% MB was decolorized because of the degradation of the substance after long exposure to sunlight. The mixed metal oxides ($EGZrO_2/EGZnO/EGFe_2O_3/HY$) photocatalyst exhibit better performance with enhance photocatalytic activity. It might be due to the catalytic performance through structural features and the interaction between the materials leads to the

277 enhancement of the contact between the surface and irradiation, as well as active species of
278 mixed metal oxides. In addition, the formation of nanosized photocatalyst increase in surface
279 area (porosity) and give the quantum effect, thus enhancing their photoreactivity properties.
280

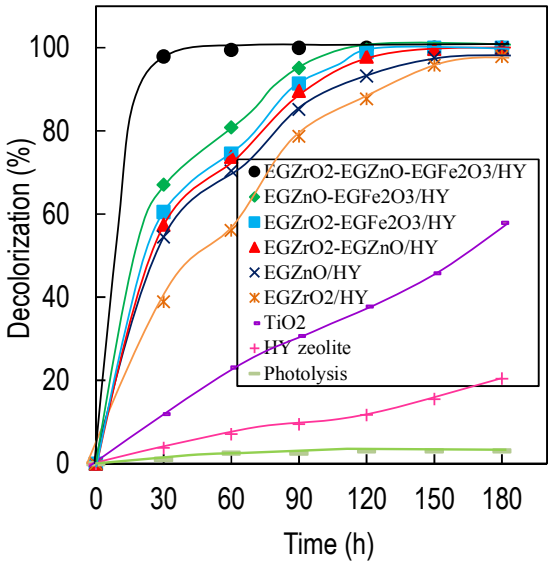

281
282 Fig. 3. Photocatalyts performance on decolorization of MB [C_{MB} = 10 mg L^{-1}, pH = 9, W = 0.38
283 g L^{-1}, t = 1 h, under sunlight irradiation]
284
285 *3.2.2. Effect of pH*
286
287 The effect of pH on the decolorization of MB using the $EGZrO_2$/EGZnO/$EGFe_2O_3$/HY
288 catalyst was studied in the pH range of 3–11 under sunlight conditions. An increase in
289 decolorization was observed from pH 3 to pH 9, but a further increase to pH 11 resulted in a
290 decrease in decolorization. The highest decolorization was obtained at pH 9 with a total
291 decolorization of 99.5%, whereas the other conditions gave 91.3%, 82.8%, 36.8%, and 21.3%
292 decolorization at pH 11, pH 7, pH 5, and pH 3, respectively. In alkaline medium, the MB cations
293 are easily attracted to the catalyst surface because of the low competition given by the abundance

of hydroxyl anions in the solution. Thus, exposure of this state to sunlight increased the formation of hydroxyl radicals and the photocatalytic reaction rate, which led to an increase in MB decolorization up to 99.5% after 1 h of contact time. However, in acidic conditions, competition between the MB cations and H^+ ions occurred, which inhibited the dyes from approaching the catalyst surface, thereby reducing the efficiency of the reaction, resulting in reduced MB decolorization. Similar results were reported in the literature regarding the photodecolorization of MB using a TiO_2/ZnS nanocomposite [26].

3.2.3. Effect of catalyst dosage

The effect of catalyst dosage was carried out with different dosages at a fixed MB concentration. An increase in decolorization was observed when the catalyst dosage was increased from 0.05 to 0.38 g L^{-1} (40.0% up to 99.5%). The increase in decolorization was most likely due to an increase in the number of active sites with higher catalyst loading contributing to an increase in the number of photons and dye molecules absorbed [23]. The most effective decolorization of MB was achieved with a catalyst dosage of 0.38 g L^{-1}, and a further increase in catalyst dosage to 1.50 g L^{-1} resulted in a decrease in decolorization (99.5% down to 47.6%). A higher particle concentration leads to greater turbidity of the suspension, which reduces light penetration and inhibits photodecolorization [27].

3.3. Investigation into biodegradability

The chemical oxygen demand (COD), total organic carbon (TOC), and five–day biochemical oxygen demand (BOD_5) for the MB solution were measured and the results are shown in Fig. 4. COD was used to investigate the amount of organic compounds that present in

the aqueous solution where the initial COD value was measured as 144 mg L^{-1}. However, this value was significantly reduced to 3 mg L^{-1} after sunlight irradiation for 1 h. The graph shows that the percentage of COD rapidly increased during the first 30 min of the reaction, which may have resulted from to the degradation of MB into two different compounds of hydroxylated and amine substituent products. The graph continuously increased until the reaction was completed to form the final products of CO_2 and H_2O [12,28]. Next, the ratio of total organic carbon (TOC/TOC_0) showed a significant decrease (0.03), which may be attributed to the fact that structured dye molecules were fragmented and converted into small organic molecules, thus enhancing mineralization during the irradiation process [29].

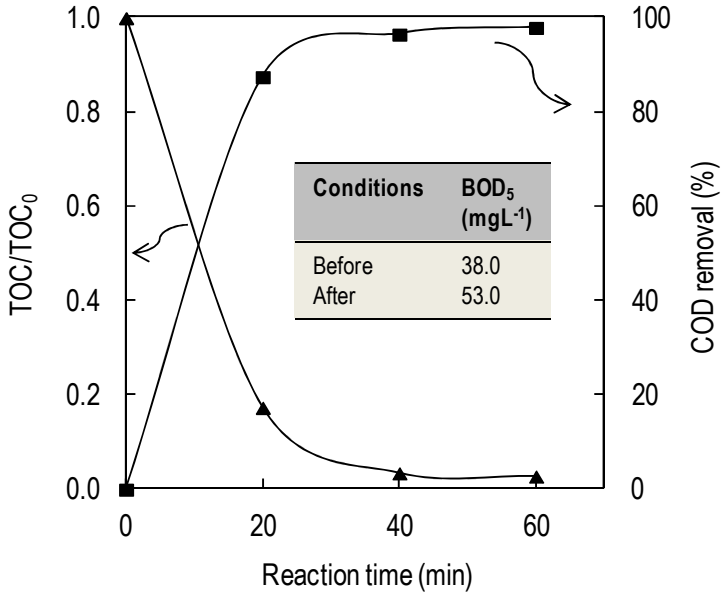

Fig. 4. The COD removal and TOC reduction levels. Insert table are its corresponding BOD_5. [C_0 = 10 mg L^{-1}, pH = 9, W = 0.38 g L^{-1}, t = 1 h, $EGZrO_2$/EGZnO/$EGFe_2O_3$/HY, under sunlight irradiation]

The five–day (BOD_5) was evaluated to measure the amount of oxygen consumed by a microorganism to degrade organic matter during a five day period. The BOD_5/COD ratio can be

used as a biodegradability index for an aqueous dye solution, and a ratio value of 0.26 was observed for the non–irradiated dye solution, indicating that the dye solution was non–biodegradable [30]. This ratio value increased up to 17.7 after irradiation for 1 h, signifying the formation of more biodegradable intermediates following photodegradation. A higher value of the BOD_5/COD ratio indicates better biodegradability [31]. In addition, the changes of the pH solution before and after the reaction were monitored. This shows that the solution reaction at pH 9 was shifted to pH 6, indicating that the MB dye was oxidized and decomposed to some extent as CO_2 and H_2O [32].

3.4. Stability of photocatalyst

To study the effect of zirconia–zinc–iron leaching into the solution, the samples were kept in the dark for 1 h, and then exposed to sunlight for 1 h before being subjected to ICP–MS. It was confirmed that photocatalysis was mainly due to the Zr, Zn, and/or Fe that exists on the catalyst surface, as the results show that no Zr, Zn, and/or Fe ions were detected (Table 2). The only trace amount of leached Zn and Fe ions (less than 1%) presence as tabulated in the table was ignored due to below the permissible level which is also reported in other studies [1,2,9,16].

Table 2. Percentage of metal detected in the solution after experimental determined by ICP–MS.

Catalysts	% metal detected in the solution		
	Zr	Zn	Fe
$EGZrO_2/EGZnO/EGFe_2O_3/HY$	-	0.12	0.34

Six cycling runs for MB decolorization were also performed to evaluate the photocatalytic activity of $EGZrO_2/EGZnO/EGFe_2O_3/HY$ (Fig. 5). The initial concentration of MB was held constant (10 mg L^{-1}) at pH 9 for the 1 h of irradiation time, and the catalyst was recycled after

filtration and calcination at 823 K for 3 h at every cycle. High MB decolorization (>90 %) could be maintained after six cycling runs and there was no obvious catalyst deactivation [1–3,16,33-35].

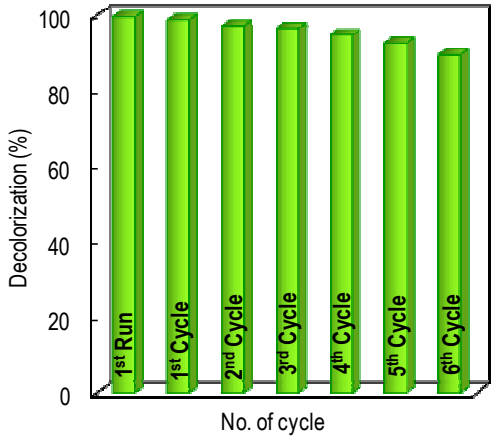

Fig. 5. Reusability of $EGZrO_2/EGZnO/EGFe_2O_3/HY$ on photocatalytic decolorization of MB [C_0 = 10 mg L^{-1}, pH = 9, W = 0.38 g L^{-1}, t = 1 h, under sunlight irradiation]

3.5. Application to other dyes

In order to study the proficiency of the $EGZrO_2/EGZnO/EGFe_2O_3/HY$ nanocomposite catalyst, various types of dyes such as malachite green (MB), congo red (CR), disperse violet (DV), and disperse blue (DB) were tested; the results are shown in Fig. 6. The initial concentration of the respective dye was held constant (10 mg L^{-1}) and was prepared using laboratory tab water, then irradiated under sunlight for 1 h of contact time. A high decolorization percentage (>80%) of various types of dye was obtained, showing the potential of these electrogenerated nanocomposite catalyst.

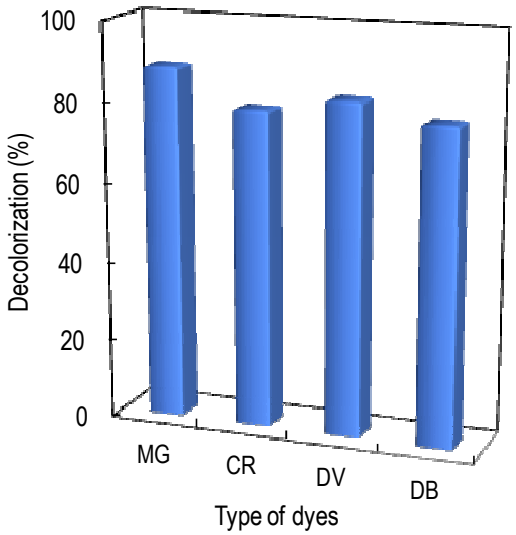

374

375 Fig. 6. Application of $EGZrO_2$/EGZnO/$EGFe_2O_3$/HY on photocatalytic decolorization of various
376 type of dyes [C_0 = 10 mg L^{-1}, pH = 9, W = 0.38 g L^{-1}, t = 1 h, under sunlight irradiation]

377

378 **3.6. Principle of band gap energy**

379

380 Modification of semiconductor metal species can increase the efficiency of photoactivity
381 the material due to improved light sensitivity. The preparation of the triple metal via
382 electrochemical method was performed, and the results show an enhanced and extendable
383 response to the visible light region (Fig. 7a). The band gap in a semiconductor material is related
384 to the absorbed wavelength range; the higher the absorption wavelength, the shorter the band gap
385 energy [36]. Therefore, the addition of more metal oxide can lower the band gap energy, and
386 consequently allow the photocatalyst to be activated by weaker energy.

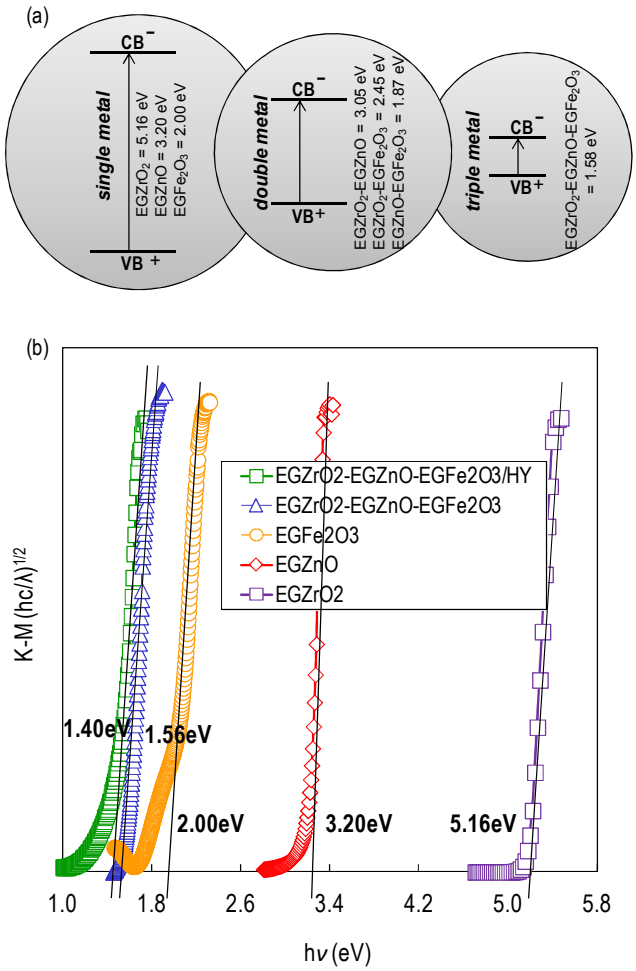

387

388 Fig. 7. (a) Schematic energy level diagram of single, double, and triple metal oxide catalyst (b)

389 the ($f_{K\text{-}M}$) vs. (hν) spectra of catalysts plot

390

391 Semiconductors such as ZrO_2, ZnO, and Fe_2O_3 can be excited by photons with appropriate

392 energy to produce the photogenerated electron or hole pairs. Electron and hole separation may

393 take place between ZrO_2, ZnO, and Fe_2O_3 in the ternary oxide, since the energy level of ZnO and

394 Fe_2O_3, both for the valence band (VB) and the conduction band (CB), correspond well within the

395 band gap of ZrO_2. When the electrons are excited, most of the electrons from the CB of ZrO_2 can

396 easily transfer to the CB of ZnO or Fe_2O_3; by this means, electron hole recombination may be

397 prevented as well [37]. According to Fig. 7b, it was verified that the band gap energy changed

significantly between $EGZrO_2$, EGZnO, $EGFe_2O_3$, $EGZrO_2$/EGZnO/$EGFe_2O_3$, and $EGZrO_2$/EGZnO/$EGFe_2O_3$/HY, at 5.16 eV, 3.20 eV, 2.00 eV, 1.56 eV, and 1.40 eV, respectively. The band gap energy was determined using the plotted Kubelka–Munk (K–M) spectrum.

The band gap energy of metal oxide semiconductors in this study is in agreement with the literature values [38]. It was found that the combination of metal oxides caused a decrease in the band gap (red shift). Similar phenomenon was also reported in the literature [39,40]. The outcome of modification showed that the band gap energy of the triple metal oxide $EGZrO_2$/EGZnO/$EGFe_2O_3$ (1.56 eV) and $EGZrO_2$/EGZnO/$EGFe_2O_3$/HY (1.40 eV) was reduced compared to single metal oxide catalyst which were 5.16 eV, 3.20 eV and 2.00 eV for $EGZrO_2$, EGZnO and $EGFe_2O_3$ catalyst, respectively.

Similar results were also reported in the literature regarding the enhancement of optical properties of photocatalysts by combination of several metal oxides [39,40]. In addition, the combination of the three metal oxides caused the reduction in total band gap (red shift) and synergistic effect that led to the enhancement of the photocatalytic performance [4-8,39,40]. The presence of Si in zeolite material might also influence the reduction of band gap of $EGZrO_2$/EGZnO/$EGFe_2O_3$/HY photocatalyst to 1.40 eV.

4. Conclusions

In this study, a new synthesis method was introduced for highly photoactive electrogenerated zirconia/zinc/iron–supported on HY zeolite ($EGZrO_2$/EGZnO/$EGFe_2O_3$/HY) nanocomposite catalyst for efficient degradation of methylene blue (MB). The excellent photoresponse of the prepared catalysts under sunlight conditions was also advantageous. An amount of 0.38 g L^{-1} 1 wt% $EGZrO_2$/1 wt% EGZnO/1 wt% $EGFe_2O_3$/HY was found to be the

optimum dosage for 10 mg L^{-1} MB, which gave 99.5% decolorization of MB after 1 h of contact time at pH 9 under sunlight irradiation. The mineralization of MB was measured by COD removal as well as BOD_5/COD and TOC/TOC_0 ratio analyses, which were found to be 97.9%, 17.7, and 0.03, respectively, after 1 h of contact time. The catalyst was still stable after six cycling runs and the leaching test showed negligible leaching effects. A high decolorization percentage (>80%) was obtained using other dyes such as malachite green (MG), congo red (CR), disperse violet (DV), and disperse blue (DB). Significantly, the simple operation, short synthesis time, high decolorization percentage of MB, and above all, may make this synthesis method an obvious choice for the preparation of various catalysts for a variety of applications.

Acknowledgement

The authors are grateful for the financial support by the Research University Grant from Universiti Teknologi Malaysia (Grant No. 01H59), the awards of UTM-RMC Postdoctoral Fellowship and UTM Zamalah Scholarship (Norzahir Sapawe), and special thanks to Associate Professor Dr Aishah Abdul Jalil and Professor Dr Sugeng Triwahyono for their supports, help and guidance throughout the research.

References

[1] N.F. Jaafar, A.A. Jalil, S. Triwahyono, M.N.M. Muhid, N. Sapawe, M.A.H. Satar, H. Asaari, *Chem. Eng. J.*, 2012, **191**, 112–122.

[2] N. Sapawe, A.A. Jalil, S. Triwahyono, R.N.R.A. Sah, N.W.C. Jusoh, N.H.H. Hairom, J. Efendi, *Appl. Catal. A: Gen.*, 2013, **456**, 144–158.

[3] A.A. Jalil, M.A.H. Satar, S. Triwahyono, H.D. Setiabudi, N.H.N. Kamarudin, N.F. Jaafar, N. Sapawe, R. Ahamad, *J. Electroanal. Chem.*, 2013, **701**, 50–58.

[4] W. Zhou, K. Liu, H. Fu, K. Pan, L. Zhang, L. Wang, C.C. Sun, *Nanotechnol.*, 2008, **19**, 1–7.

[5] M.J. Height, S.E. Pratsinis, O. Mekasuwandumrong, P. Praserthdam, *Appl. Catal. B: Environ.*, 2006, **63**, 305–312.

[6] X. Yang, C. Cao, L. Erickson, K. Hohn, R. Maghirang, L. Klabunde, *Appl. Catal. B: Environ.*, 2009, **91**, 657–662.

[7] J.H. Sun, S.Y. Dong, J.L. Feng, X.J. Yin, X.C. Zhao, *J. Mol. Catal. A: Chem.*, 2011, **335**, 145–150.

[8] W. Zhao, L. Feng, R. Yang, J. Zheng, X. Li, *Appl. Catal. B: Environ.*, 2011, **103**, 181–189.

[9] N. Sapawe, A.A. Jalil, S. Triwahyono, *Chem. Eng. J.*, 2013, **225**, 254–265.

[10] W. Zhang, K. Wang, Y. Yu, H. He, *Chem. Eng. J.*, 2010, **163**, 62–67.

[11] Z.M. El–Bahy, M.M. Mohamed, F.I. Zidan, M.S. Thabet, *J. Hazard. Mater.*, 2008, **153**, 364–371.

[12] A. Nezamzadeh–Ejhieh, S. Hushmandrad, *Appl. Catal. A: Gen.*, 2010, **388**, 149–159.

[13] H. Chen, A. Matsumoto, N. Nishimiya, K. Tsutsumi, *Colloids Surf. A*, 1999, **157**, 295–305.

[14] X. Liu, K.K. Iu, J.K. Thomas, *J. Chem. Soc., Faraday Trans.*, 1993, **89**, 1861–1865.

[15] M. Aleksic, H. Kusic, N. Koprivanac, D. Leszczynska, A. L. Bozic, *Desalination*, 2010, **257**, 22–29.

[16] N. Sapawe, A.A. Jalil, S. Triwahyono, S.H. Adam, N.F. Jaafar, M.A.H. Satar, *Appl. Catal. B: Environ.*, 2012, **125**, 311–323.

[17] Y.C. Zhang, L. Yao, G. Zhang, D.D. Dionysiou, J. Li, X. Du, *Appl. Catal. B: Environ.*, 2014, **144**, 730–738.

[18] N.W.C. Jusoh, A.A. Jalil, S. Triwahyono, H.D. Setiabudi, N. Sapawe, M.A.H. Satar, A.H, Karim, N.H.N. Kamarudin, R. Jusoh, N.F. Jaafar, N. Salamun, J. Efendi, *Appl. Catal. A: Gen.*, 2013, **468**, 276–287.

[19] N. Chandra, D.K. Singh, M. Sharma, R.K. Upadhyay, S.S. Amritphale, S.K. Sanghi, *J. Colloid Interface Sci.*, 2010, **342**, 327–332.

[20] L.Y. Zhu, X.Q. Wang, G.H. Zhang, Q. Ren, D. Xu, *Appl. Catal. B: Environ.*, 2011, **103**, 428–435.

[21] K. Hayat, M.A. Gondal, M.M. Khaled, S. Ahmed, A.M. Shemsi, *Appl. Catal. A: Gen.*, 2011, **393**, 122–129.

[22] Q. Chang, J.E. Zhou, Y. Wang, G. Meng, *Adv. Powder Technol.*, 2009, **20**, 371–374.

[23] D.P. Das, N. Baliarsingh, K.M. Parida, *J. Mol. Catal. A: Chem.*, 2007, **261**, 254–261.

[24] C.J. Lucio–Ortiz, J.R. De la Rosa, A. Hernandez–Ramirez, E.M. Lopez–Cuellar, G. Beltran–Perez, R.D.C.M. Guardiola, C.D. Pedroza–Solis, *Colloids Surf. A: Physicochem. Eng. Asp.*, 2010, **371**, 81–90.

[25] R. Chatti, S.S. Rayalu, N. Dubey, N. Labhsetwar, S. Devotta, *Sol. Energy Mater. Sol. Cells*, 2007, **91**, 180–190.

[26] A. Franco, M.C. Neves, M.M.L. Mobteiro, *J. Hazard. Mater.*, 2009, **161**, 545–550.

[27] E. Bizani, K. Fytianos, I. Poulios, V. Tsiridis, *J. Hazard. Mater.*, 2006, **136**, 85–94.

[28] A. Houas, H. Lachheb, M. Ksibi, E. Elaloui, C. Guillard, J.M. Herrmann, *Appl. Catal. B: Environ.*, 2001, **31**, 145–157.

[29] J. Paul, K.P. Rawat, K.S.S. Sarma, S. Sabharwal, *Appl. Radiat. Isot.*, 2011, **69**, 982–987.

[30] H. Chun, W. Yizhong, *Chemosphere*, 1999, **39**, 2107–2115.

[31] K. Swaminathan, K. Pachhade, S. Sandhya, *Desalination*, 2005, **186**, 155–164.

[32] X. Li, K. Lv, K. Deng, J. Tang, R. Su, J. Sun, L. Chen, *Mater. Sci. Eng. B*, 2009, **158**, 40–47.

[33] N. Sapawe, A.A. Jalil, S. Triwahyono, M.I.A. Shah, R. Jusoh, N.F.M. Salleh, B.H. Hameed, A.H. Karim, *Chem. Eng. J.*, 2013, **229**, 388–398.

[34] R. Jusoh, A.A. Jalil, S. Triwahyono, A. Idris, S. Haron, N. Sapawe, N.F. Jaafar, N.W.C. Jusoh, *Appl. Catal. A: Gen.*, 2014, **469**, 33–44.

[35] A.A. Jalil, S. Triwahyono, N. Sapawe, I.H. Ahmed, M.A.A. Aziz, *Desalin. Water Treat.*, 2014, 1–15.

[36] Y. Kim, J. Lee, H. Jeong, Y. Lee, M.H. Um, K.M. Jeong, M.K. Yeo, M. Kang, *J. Ind. Eng. Chem.*, 2008, **14**, 396–400.

[37] B. Neppolian, Q. Wang, H. Yamashita, H. Choi, *Appl. Catal. A: Gen.*, 2007, **333**, 264–271.

[38] J. Portier, H.S. Hilal, I. Saadeddin, S.J. Hwang, M.A. Subramanian, G. Campet, *Prog. Solid State Chem.,* 2004, **32**, 207–217.

[39] M. Pelaez, N.T. Nolan, S.C. Pillai, M.K. Seery, P. Falaras, A.G. Kontos, P.S.M. Dunlop, J.W.J. Hamilton, J.A. Byrne, K. O'Shea, M.H. Entezari, D.D. Dionysiou, *Appl. Catal. B: Environ*., 2012, **125**, 331–349.

[40] C. Han, M. Pelaez, V. Likodimos, A.G. Kontos, P. Falaras, K. O'Shea, D.D. Dionysiou, *Appl. Catal. B: Environ*., 2011, **107**, 77–87.